Analysis of dynamics in a parametrically damped pendulum

Fa-Gen Xie and Wei-Mou Zheng
Institute of Theoretical Physics, Academia Sinica, 100080 Beijing, China
(Received 5 April 1993; revised manuscript received 5 October 1993)

For the parametrically damped pendulum exhibiting chaotic transients, the critical values of various parameters are determined from the calculation of Floquet multipliers at finite truncations of the harmonics. The transient long-term behavior is related to a Floquet multiplier near zero. Dynamical foliations are used to understand basin boundaries and attractor remnants.

PACS number(s): 05.45.+b

I. INTRODUCTION

Transient phenomena are diverse in chaotic dynamics. In an early work of Levinson on the Van der Pol equation [1] the complex transient response due to the existence of competing attractors was studied. Another type is repetitive bursts of chaotic motion known as intermittency [2]. When a strange attractor collides with an unstable periodic orbit (or its stable manifold), a sudden qualitative change accompanied by a transient behavior also occurs, which is called a crisis [3].

Generally, a long-term transient is related to an orbit of critical stability, the Lyapunov exponent of which vanishes. A simple example is the "critical slowing down" at a period-doubling bifurcation point. For the three types of intermittency studied in Ref. [2] the orbits of critical stability are simple periodic orbits. For the crisis such orbits are orbits of heteroclinic or homoclinic tangency. The orbit of critical stability is essential to understanding the transient dynamics of systems.

Recently, the transient chaos in a parametrically damped pendulum was studied numerically by using the cell-mapping method [4]. In this paper we present some analytic discussions of the problem. The model considered in Ref. [4] is described by

$$\frac{d^2\theta}{dt^2}+Q^{-1}[1+\epsilon\sin(\Omega t)]\frac{d\theta}{dt}+\sin\theta=0\ , \tag{1}$$

where parameter $Q=18.33$ [4], but the other two, ϵ and Ω, are adjustable. The equation may be written as

$$\omega^2\frac{d^2\theta}{dt^2}+q[1+\varepsilon\sin(2t)]\frac{d\theta}{dt}+\sin\theta=0 \tag{2}$$

by the transformation

$$t\rightarrow\frac{2t}{\Omega}\ ,\quad \omega=\frac{\Omega}{2}\ ,\quad q=\frac{\Omega}{2Q}\ ,\quad \varepsilon=\frac{\epsilon}{2}\ , \tag{3}$$

where the factor 2 in the argument of the sine function has been introduced for convenience. This equation always possesses the particular solution $\theta=\dot\theta=0$, which, however, need not be stable against small perturbations. The transient dynamics associated with this orbit was studied in Ref. [4]. The stability boundaries of this stationary solution were discussed with the method of Lindstedt-Poincaré perturbation in Ref. [5], where well-behaved dynamical properties of the system were found.

In this paper we shall perform a different analysis of the dynamics of the system. In the next section we determine the stability boundaries of the orbit $\dot\theta=\theta=0$ based on the Floquet theorem. In Sec. III we use a Floquet multiplier to describe the transient lifetime. In Sec. IV we construct basin boundaries and attractor remnants with invariant manifolds. We then briefly discuss the bifurcation behavior of the system in Sec. V. Our analysis uses a geometrical method based on dynamical foliations which are a generalization of invariant manifolds. This method provides a better understanding of the dynamics than the intuitive cell-mapping method of the phase space. Finally, in the last section we make a few concluding remarks.

II. STABILITY BOUNDARIES OF THE STATIONARY SOLUTION

The linearized equation for a perturbation ξ around the solution $\dot\theta=\theta=0$ reads

$$\omega^2\ddot\xi+q(1+\varepsilon\sin2t)\dot\xi+\xi=0\ . \tag{4}$$

The boundary of stability may be determined from the existence of a periodic solution for ξ. In Ref. [5] the periodic solution of ξ was determined with the method of Lindstedt-Poincaré perturbation. Here we use the Floquet theorem to treat the same problem. At the stability boundaries a Floquet multiplier must vanish. Thus we may assume that

$$\xi=A_0+\sum_{n=1}^{\infty}(A_n\cos nt+B_n\sin nt)\ . \tag{5}$$

Inserting relation (5) into Eq. (4), by balancing harmonics, we find that

$$\begin{aligned}&(1-n^2\omega^2)A_n+nqB_n\\&\qquad+q\varepsilon[(n-2)A_{n-2}-(n+2)A_{n+2}]=0\ ,\\&(1-n^2\omega^2)B_n-nqA_n\\&\qquad+q\varepsilon[(n-2)B_{n-2}-(n+2)B_{n+2}]=0\ ,\end{aligned} \tag{6}$$

where we have made the convention $A_{-n}=A_n$ and

$B_{-n}=-B_n$. It can be seen that the solution to Eq. (6) decomposes into two classes, one involving odd n's, and another involving even n's. No nontrivial solution exists for the latter, so we consider only odd n. For the lowest-order approximation we truncate Eq. (6) at $n=1$. We then have the following two equations:

$$\begin{aligned}(1-\omega^2-q\varepsilon)A_1+qB_1=0\ ,\\ (1-\omega^2+q\varepsilon)B_1-qA_1=0\ .\end{aligned} \tag{7}$$

The existence of a nontrivial solution requires the determinant of the coefficients to vanish:

$$\begin{vmatrix}1-\omega^2-q\varepsilon & q\\ -q & 1-\omega^2+q\varepsilon\end{vmatrix}=0\ , \tag{8}$$

which gives

$$\varepsilon_c^{(1)}=q^{-1}\sqrt{(1-\omega^2)^2+q^2}\ . \tag{9}$$

The next approximation is obtained from the truncation at $n=3$. From Eq. (6) four equations for A_1, A_3, B_1, and B_3 similar to Eq. (7) may be derived, and the condition for the existence of a nontrivial solution becomes

$$\begin{vmatrix}1-\omega^2-q\varepsilon & q & -3q\varepsilon & 0\\ -q & 1-\omega^2+q\varepsilon & 0 & -3q\varepsilon\\ q\varepsilon & 0 & 1-9\omega^2 & 3q\\ 0 & q\varepsilon & -3q & 1-9\omega^2\end{vmatrix}=0\ , \tag{10}$$

or

$$\begin{aligned}9(q\varepsilon)^4-[(1-9\omega^2)^2+3(3q)^2-6(1-\omega^2)(1-9\omega^2)](q\varepsilon)^2\\ +[(1-\omega^2)^2+q^2][(1-9\omega^2)^2+(3q)^2]=0\ ,\end{aligned} \tag{11}$$

from which $\varepsilon_c^{(2)}$, a higher approximation of the critical value for ε, may be found. The result is shown in Fig. 1, which is very close to the curve determined in Ref. [4] by directly integrating Eq. (1).

For $\Omega=1.5$, the value considered in Ref. [4], we have calculated ϵ_c for successive truncations. The results are

$\epsilon_c=21.48$ for the truncation at $n=1$,

$\epsilon_c=17.0826$ at $n=3$,

$\epsilon_c=17.1818$ at $n=5$,

$\epsilon_c=17.180\,599\,6$ at $n=7$.

We have also obtained $\epsilon_c=17.1806$ by numerically computing the eigenvalues, which are $-1.000\,041\,96$ and $-0.795\,850\,40$ at $\epsilon=\epsilon_c$. Thus we estimate that $\epsilon_c=17.1806$, which is an improvement on the value $\epsilon_c=17.2$ given in Ref. [4].

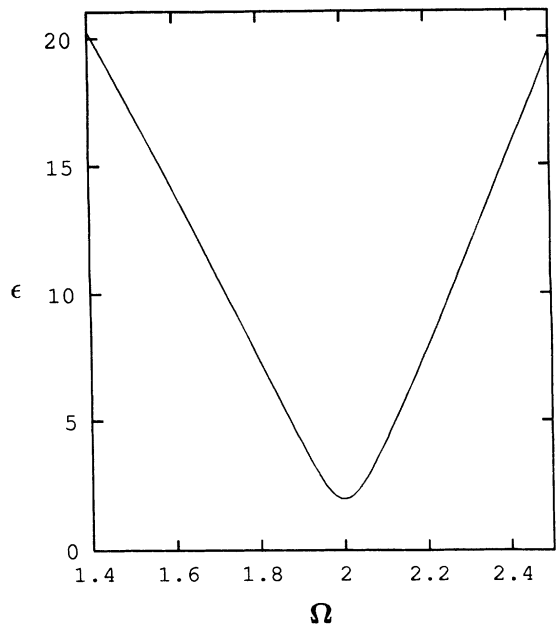

FIG. 1. The boundary of stability of the solution $\dot{\theta}=\theta=0$ for the parametrically damped pendulum.

The negative sign of the eigenvalues involving critical stability indicates that the period of the solution is doubled with respect to that of the parametric term. By introducing the factor 2 into Eq. (2), this period-doubled solution can be readily treated. Compared with the Lindstedt-Poincaré perturbation method the above method is more convenient for obtaining higher-order results. In the next section we shall see that the same method can be extended to deal with the transient phenomena.

III. TRANSIENT LIFETIME

When ϵ is not exactly set at ϵ_c, from the Floquet theorem, instead of the form (5) we generally have

$$\xi=e^{\mu t}\sum_{n=1}^{\infty}(A_n\cos nt+B_n\sin nt)\ . \tag{12}$$

where μ is a Floquet multiplier. Correspondingly, the equations of harmonic balance are now

$$\begin{aligned}[\omega^2(\mu^2-n^2)+1+q\mu]A_n+n(2\mu+q)B_n+q\varepsilon[\mu(B_{n+2}-B_{n-2})+(n-2)A_{n-2}-(n+2)A_{n+2}]=0\ ,\\ [\omega^2(\mu^2-n^2)+1+q\mu]B_n-n(2\mu+q)A_n+q\varepsilon[\mu(A_{n-2}-A_{n+2})+(n-2)B_{n-2}-(n+2)B_{n+2}]=0\ .\end{aligned} \tag{13}$$

When making the truncation at $n=3$, we obtain

$$M(\mu,\varepsilon)\equiv\begin{vmatrix}1+(\mu^2-1)\omega^2+q\mu-q\varepsilon & 2\mu+q+\mu q\varepsilon & -3q\varepsilon & \mu q\varepsilon\\ -(2\mu+q)+\mu q\varepsilon & 1+(\mu^2-1)\omega^2+q\mu+q\varepsilon & -\mu q\varepsilon & -3q\varepsilon\\ q\varepsilon & -\mu q\varepsilon & 1+(\mu^2-9)\omega^2+q\mu & 3(2\mu+q)\\ \mu q\varepsilon & q\varepsilon & -3(2\mu+q) & 1+(\mu^2-9)\omega^2+q\mu\end{vmatrix}=0\ , \tag{14}$$

which, for $\mu=0$, reduces to Eq. (10). Up to the linear term of μ, we may write Eq. (14) as

$$M_\varepsilon(0,\varepsilon_c)(\varepsilon-\varepsilon_c)+M_\mu(0,\varepsilon_c)\mu=0 , \tag{15}$$

where

$$M_\varepsilon(0,\varepsilon_c)=\left.\frac{\partial M(\mu,\varepsilon)}{\partial\varepsilon}\right|_{\mu=0,\varepsilon=\varepsilon_c} ,$$

$$M_\mu(0,\varepsilon_c)=\left.\frac{\partial M(\mu,\varepsilon)}{\partial\mu}\right|_{\mu=0,\varepsilon=\varepsilon_c} .$$

Generally, both $M_\varepsilon(0,\varepsilon_c)$ and $M_\mu(0,\varepsilon_c)$ are not vanishing, so that

$$\mu\propto\epsilon-\epsilon_c . \tag{16}$$

The argument does not rely on the truncation made, so relation (16) is generic. We have numerically computed Floquet multipliers at $\Omega=1.5$. The branch to which $\mu_c=0$ belongs is shown in Fig. 2.

Around ϵ_c the long-term behavior of the system should be described by the Floquet multiplier close to zero. As in Refs. [4] and [5], we choose the Poincaré section at $t=2n\pi/\Omega$ for Eq. (1). In the Poincaré section two direction fields [6] may be constructed as follows, one for the forward dynamics, and the other for the backward. Consider a cluster of points on a circle surrounding the initial point of an orbit. In general, after a number of iterations of the forward Poincaré map, the circle is stretched into an ellipse around some final point due to the dynamical instability. If we fix this final point and increase backwards the length of the orbit, the major axes of such ellipses approach a limit direction, which may be called the backward direction of that given point. For most cases of interest there exists a field of the backward direction [6]. The integral curves of the fields form the backward foliations, which, for an unstable periodic orbit, are just the unstable invariant manifolds. Similarly, we can construct another class of foliations for the backward Poincaré map. These two classes of dynamical foliations play an important role in the construction of symbolic dynamics for two-dimensional maps [7]. Generally, a segment of a forward foliation will map to a contracted segment on another forward foliation, and a segment of a backward foliation will be expanded.

When ϵ is very close to but still a little smaller than ϵ_c, one of the two eigenvalues has an absolute value only a little less than 1, and another has an absolute value much less than 1. The latter is associated with the forward foliations. Points near the origin $\dot\theta=\theta=0$ on the Poincaré section, moving quickly along the forward foliations, approach the backward foliation passing through the origin. The backward foliation, being weakly contractive, forms a "bottleneck" in the flow, as shown in Fig. 3. The long-term behavior is governed by the eigenvalue with its absolute value close to 1 or by the Floquet multiplier μ corresponding to it. Thus it is reasonable to claim that the mean transient lifetime T is scaled as

$$T\sim\mu^{-1}\sim|\epsilon-\epsilon_c|^{-1} . \tag{17}$$

Taking the reciprocal of the Floquet multiplier μ as a measure of the mean transient lifetime, we plot it as a function of ϵ in Fig. 4, which is consistent with the numerical finding of Ref. [4] (cf. Fig. 9 there).

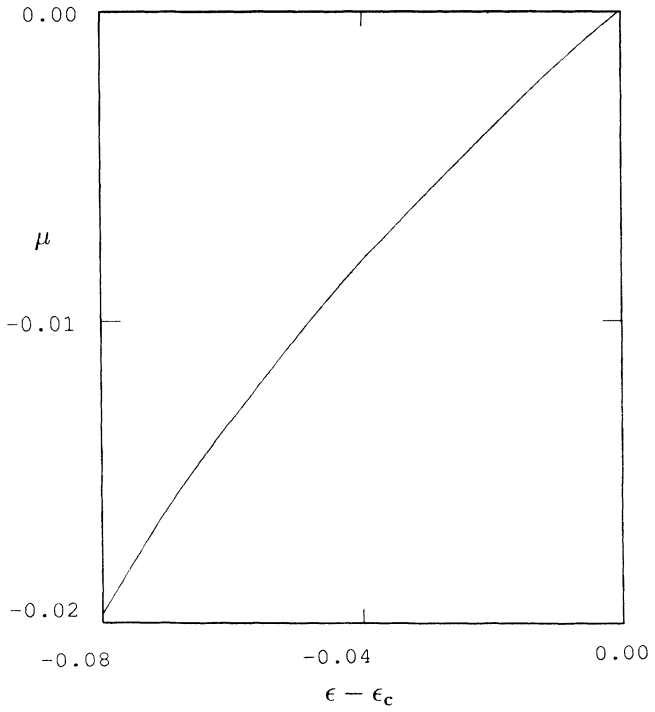

FIG. 2. Plot of the Floquet multiplier μ vs $\epsilon-\epsilon_c$.

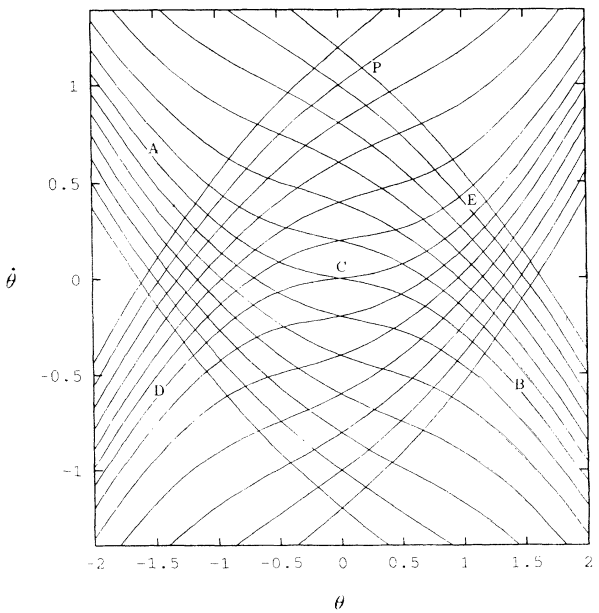

FIG. 3. Some forward and backward foliations near the origin $\theta=\dot\theta=0$ at $\epsilon=17.10$. The origin is marked by the letter C. The forward and backward foliations passing through the origin are curves ACB and ECD, respectively. The point P approaches E on the backward foliation ECD rather quickly, and then slowly reaches C, the stable fixed point.

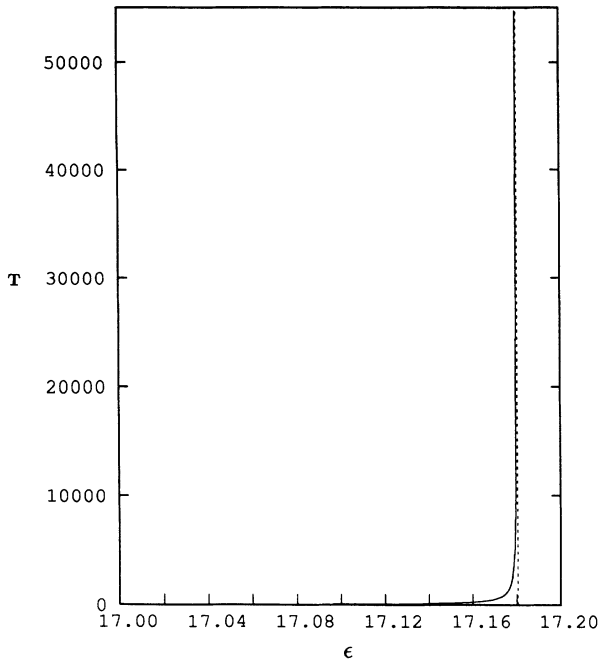

FIG. 4. The reciprocal of the Floquet multiplier plotted as a function of ϵ for $\Omega=1.50$.

IV. BASIN BOUNDARIES AND ATTRACTOR REMNANTS

It is well known that a basin is related to forward foliations, while an attractor is related to backward foliations. Some forward and backward foliations are shown in Figs. 5 and 6 for ϵ above and below ϵ_c, respectively. Figures 5(a) and 5(b) are obtained by taking 5000 points on a segment of length about 0.01 along the stable and unstable eigenvectors of the fixed point $(\theta,\dot{\theta})=(0.0,0.0)$, and then iterating them backwards and forwards, respectively. When generating Fig. 6(a), we start from 20 points on the line $\theta=\pi$, and calculate the forward dynamical direction field directly step by step to find integral curves for foliations. To guarantee the accuracy of integration, the step size is adjustable as follows. At a given point P we calculate the dynamical direction as described in the preceding section, and pick up a point P' along that direction at a distance of the current step size away from point P. Then we determine the direction at point P' and the angle formed by the two directions at points P and P'. If the tangent of the angle is between ± 0.02, we accept point P' as a new point of the foliation curve; otherwise we reduce the step by half, and continue the process. When the step size is less than 10^{-4}, we always take a step, no matter what the angle is. After a step is made, we double the step size to accelerate the calculation. For every initial point we integrate the foliation curve until it reaches the borders $\theta=\pm\pi$ and $\dot{\theta}=\pm 10$, or until the total number of points reaches 1000, according to whichever comes first. When generating Fig. 6(b) we determine the backward direction at point $(\theta,\dot{\theta})=(3.0,0.0)$, take points near it in that direction, and iterate them forward. Foliations usually change smoothly with parameters even at a sudden change of attractor. For $\epsilon<\epsilon_c$ (Fig. 6) the long-term behavior is mainly governed by the backward foliation. Thus backward foliations represent the remnant of the attractor. When the value of ϵ crosses the critical ϵ_c from above, a strange attractor as a set of backward foliations gently becomes an attractor remnant due to the loss of stability.

Below the left edge of the V-shaped region in Fig. 1 there may coexist four attractors: the stationary solution $\dot{\theta}=\theta=0$, one oscillating solution, and two rotating solutions. The former two are a bistable pair, accompanied by an unstable orbit of period 2 [5]. These three orbits

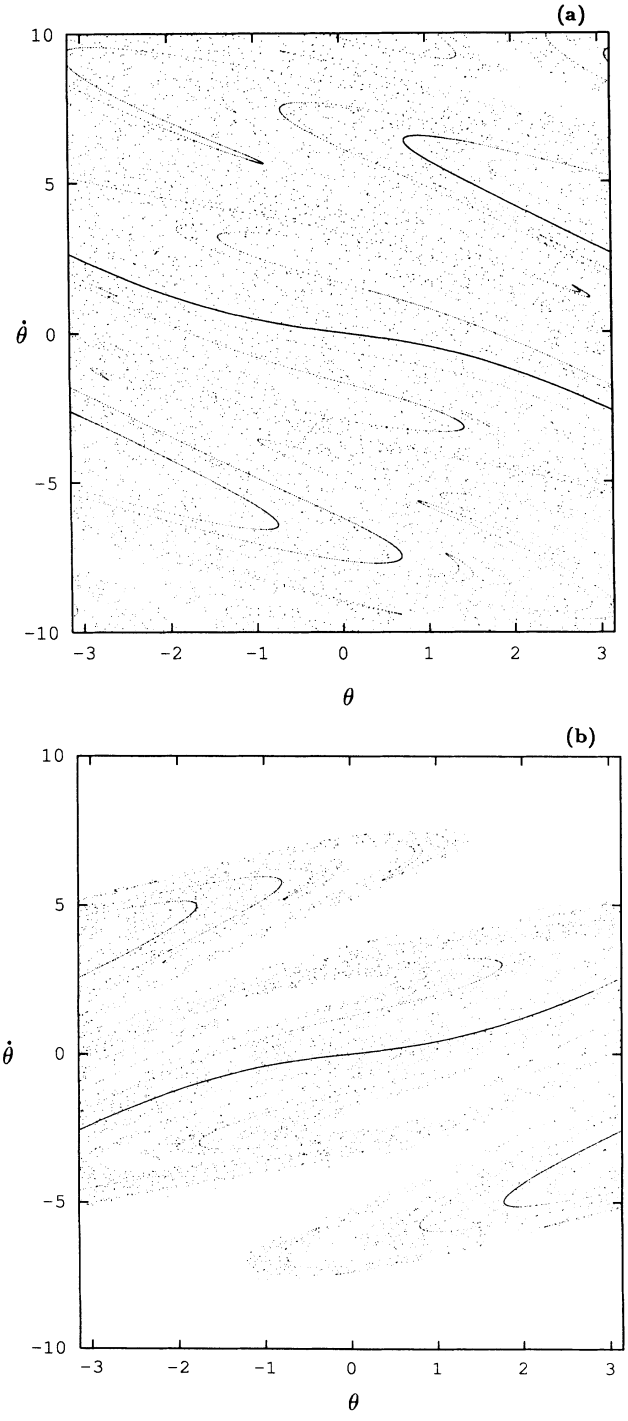

FIG. 5. Some forward foliations (a) and backward foliations (b) for $\epsilon=20.00$ and $\Omega=1.5$.

correspond to a cubic-type curve in the bifurcation diagram. The stable manifold of the unstable orbit forms the boundary of basins for the two bistable solutions. This basin boundary is shown in Fig. 7(a) for parameters $\epsilon=6.0$, $\Omega=1.7$, and $Q=18.33$, which is generated from a segment of the stable manifold of the unstable orbit indicated by open circles. When the unstable orbit (or its stable manifold) collides with the stationary solution $\dot{\theta}=\theta=0$, the latter will lose its stability and become unstable.

The two rotating or running solutions are each accompanied by an unstable rotating one. The stable manifolds of the two unstable rotating solutions indicated by open circles are shown in Fig. 7(b) at the same parameters as

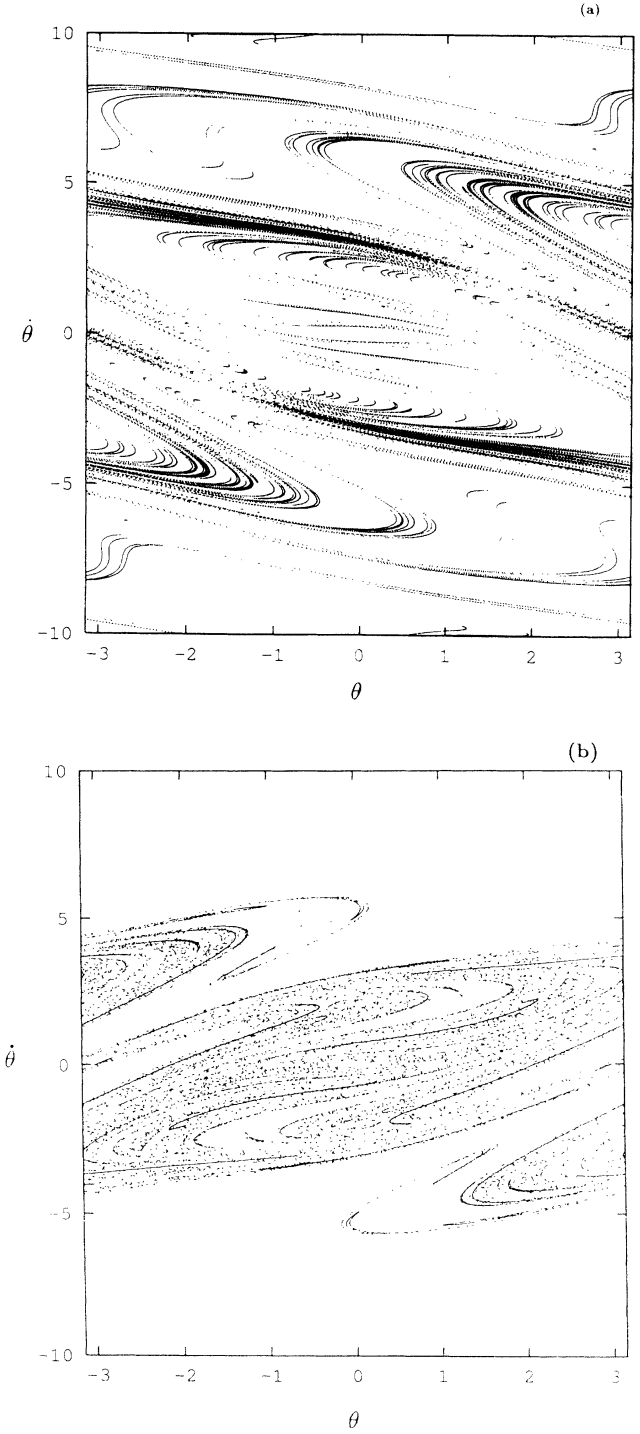

FIG. 6. Some forward foliations (a) and backward foliations (b) for $\epsilon=15.00$ and $\Omega=1.5$. Backward foliations represent the remnant of the destroyed attractor.

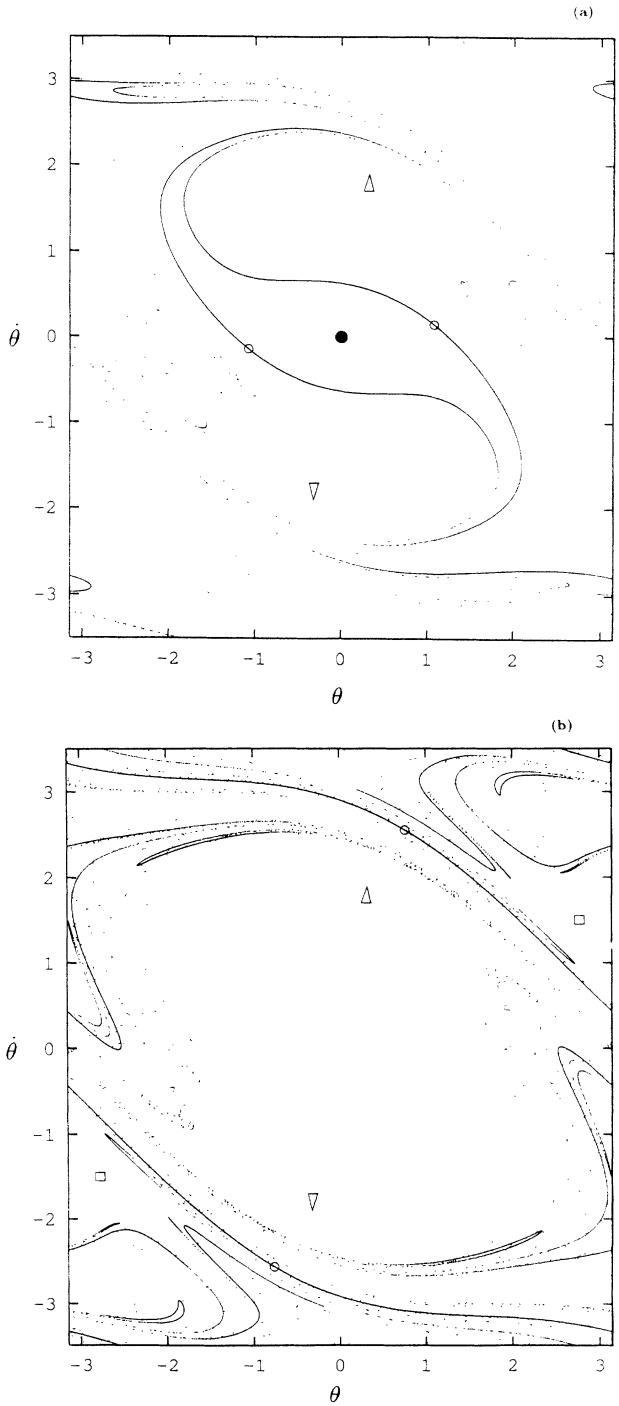

FIG. 7. The stable manifolds of unstable periodic orbits at $\epsilon=6.0$, $\Omega=1.7$, and $Q=18.33$. The solid circle, triangles, rectangles, and open circles indicate the stable orbit $\dot{\theta}=\theta=0$, the oscillating solution, two rotating solutions, and the unstable orbits, respectively. (a) The stable manifolds of the unstable oscillating orbit of period 2. (b) The stable manifolds of the two unstable rotating orbits of period 1.

those in Fig. 7(a). They form the boundaries between basins for the rotating and oscillating solutions. The stable manifolds of the two unstable rotating orbits tangle with that of the unstable oscillating orbit, forming a complicated structure in the phase space of the Poincaré intersection. Our figures of dynamical foliations agree with the numerical results of the cell mapping method in Ref. [4]. The construction of the basin boundary directly from the forward foliations deepens our understanding of the dynamics.

V. BIFURCATION BEHAVIOR

The bifurcation behavior of the parametrically damped pendulum was studied in Refs. [4] and [5]. The segment with $\Omega > 2$ of the V-shaped stability boundary was identified as a Hopf bifurcation. Along the line $\Omega = 2.40$ in Fig. 1 we calculate the two eigenvalues for point $\dot{\theta} = \theta = 0$, which are shown in Fig. 8. In that parameter region both eigenvalues are real. There is no evidence for a Hopf bifurcation which was claimed in Refs. [4] and [5]. The bifurcation is just the usual period-doubling bifurcation.

In Ref. [5] the left boundary of parameter region for chaotic motion with $\Omega < 2$ was determined by Lyapunov exponents. The routes to chaos were categorized as an inverse boundary crisis for $\Omega < 1.66$ and a period-doubling route for $\Omega > 1.66$. We calculate the stability boundaries for the symmetric and asymmetric oscillating orbits of period 2, which are shown in Fig. 9. The stability boundaries of orbits with period 4 and 8 are too close to that of the asymmetric orbit of period 2 to be clearly seen in the figure. In Fig. 9 we also show the stability boundaries for the rotation orbits of period 2 and 4. The results indicate that along the boundary of the chaotic region for $\Omega > 1.66$ a period-doubling route does indeed occur.

At the whole left branch of the V-shaped stability boundary the stationary orbit $\dot{\theta} = \theta = 0$ always loses its stability by colliding with the unstable orbit of period 2. When viewing the discrete map in the Poincaré section by sampling at $t = 4n\pi/\Omega$, the bifurcation may be classified as a subcritical pitchfork bifurcation. There is no significant difference concerning the loss of stability for the stationary orbit above and below $\Omega = 1.66$. The difference in the dynamics is where the orbit is attracted to after losing its stability. While for $\Omega > 1.66$ the attractor is trivial, for $\Omega < 1.66$ it is generally nontrivial. Since a crisis is characterized by an orbit of homoclinic or heteroclinic tangency, as mentioned above, there is no evidence for an inverse boundary crisis.

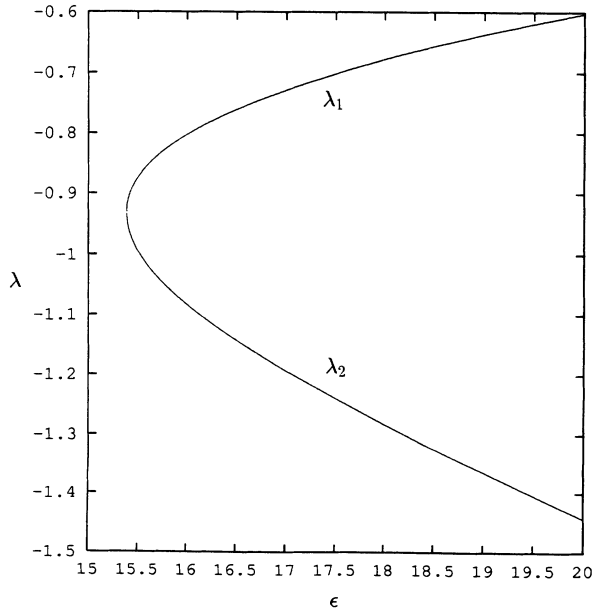

FIG. 8. Plot of eigenvalues λ_1 and λ_2 vs ϵ at $\Omega = 2.4$ and $Q = 18.33$.

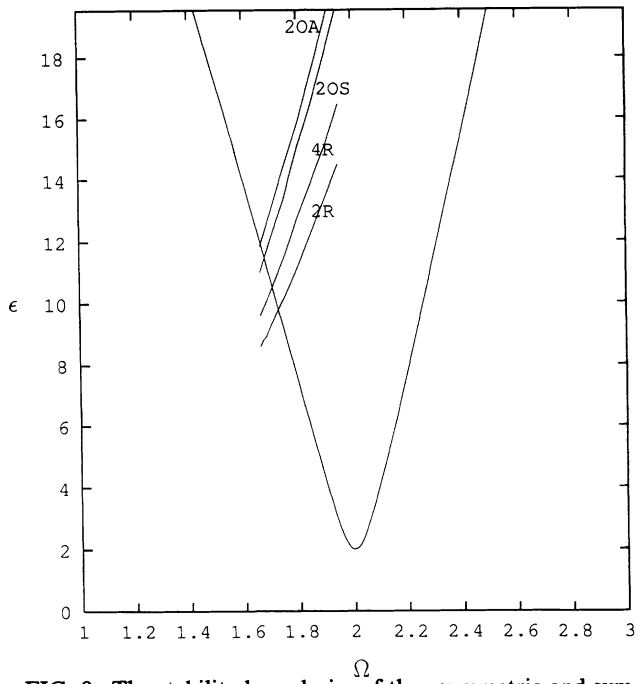

FIG. 9. The stability boundaries of the asymmetric and symmetric oscillating solutions of period 2 and those of the rotating solutions of period 4 and 2, marked by 2OA, 2OS, 4R, and 2R, respectively.

VI. CONCLUSION

We have determined the stability boundary of the stationary orbit $\dot{\theta} = \theta = 0$ by the Floquet theorem. The transient long-term behavior is closely related to a Floquet multiplier near zero, which has been taken as a measure of the lifetime. We have used dynamical foliations to understand basin boundaries and attractor remnants. Dynamical foliations are an extension of invariant manifolds, directly reflect the geometrical structure of dynamics, and thus give a better understanding of the dynamics than the cell-mapping method.

We have also discussed the bifurcation behavior of the system. For $\epsilon \gg 1$, Eq. (1) may be approximated by

$$\frac{d^2\theta}{dt^2} + Q^{-1}\epsilon \sin(\Omega t)\frac{d\theta}{dt} + \sin\theta = 0 \ .$$

Instead of two parameters Q and ϵ, the combination $Q^{-1}\epsilon$ is essential, and the system is then insensitive to damping.

ACKNOWLEDGMENT

This work was partially supported by the CNSF, China.

[1] N. Levinson, Ann. Math. **50**, 127 (1949).
[2] Y. Pomeau and P. Manneville, Commun. Math. Phys. **74**, 189 (1980).
[3] C. Grebogi, E. Ott, and J. A. Yorke, Phys. Rev. Lett. **48**, 1507 (1982).
[4] J. A. Blackburn, H. J. T. Smith, and D. E. Edmundson, Phys. Rev. A **45**, 593 (1992); H. J. T. Smith and J. A. Blackburn, *ibid.* **40**, 4708 (1989).
[5] B. Wu and J. A. Blackburn, Phys. Rev. A **45**, 7030 (1992).
[6] J. M. Greene, in *Long-Time Prediction in Nonlinear Dynamics,* edited by W. Horton, L. Reichl, and V. Szebehely (Wiley, New York, 1983); Y. Gu, Phys. Lett. **124A**, 340 (1987).
[7] W. M. Zheng, Chaos Solitons Fractals **2**, 461 (1992); H. Zhao and W. M. Zheng, Commun. Theor. Phys. (Beijing) **19**, 21 (1993).